Understanding the effect of iodide ions on the morphology of gold nanorods

Reference:

Amini Mozhgan, Altantzis Thomas, Lobato Hoyos Ivan Pedro, Grzelczak Marek, Sánchez-Iglesias Ana, Van Aert Sandra, Liz-Marzán Muis M., Partoens Bart, Bals Sara, Neyts Erik.- Understanding the effect of iodide ions on the morphology of gold nanorods
Particle and particle systems characterization - ISSN 0934-0866 - 35:8(2018), 1800051
Full text (Publisher's DOI): https://doi.org/10.1002/PPSC.201800051
To cite this reference: https://hdl.handle.net/10067/1529980151162165141

DOI: 10.1002/((please add manuscript number))
Article type: Full paper

Understanding the Effect of Iodide Ions on the Morphology of Gold Nanorods

Mozhgan N. Amini, Thomas Altantzis, Ivan Lobato, Marek Grzelczak, Ana Sánchez-Iglesias, Sandra Van Aert, Luis M. Liz-Marzán, Bart Partoens, Sara Bals and Erik C. Neyts**

Dr. M. N. Amini, Prof. Dr. E. C. Neyts
Department of Chemistry, PLASMANT Research Group, University of Antwerp
Universiteitsplein 1, B-2610 Wilrijk-Antwerp, Belgium
E-mail: erik.neyts@uantwerpen.be

Dr. T. Altantzis, Dr. I. Lobato, Prof. Dr. S. Van Aert, Prof. Dr. S. Bals
Electron Microscopy for Materials Research (EMAT), University of Antwerp
Groenenborgerlaan 171, 2020 Antwerp, Belgium
E-mail: sara.bals@uantwerpen.be

A. Sánchez-Iglesias, Prof. Dr. L. M. Liz-Marzán
Bionanoplasmonics Laboratory, CIC biomaGUNE
Paseo de Miramón 182, 20014 Donostia - San Sebastian, Spain

Dr. M. Grzelczak
Donostia International Physics Center
Paseo de Manuel Lardizabal 4, 20018 Donostia - San Sebastian, Spain

Dr. M. Grzelczak, Prof. Dr. L. M. Liz-Marzán
Ikerbasque, Basque Foundation for Science
48011 Bilbao, Spain

Prof. Dr. Bart Partoens
Condensed Matter Theory, University of Antwerp
Groenenborgerlaan 171, 2020 Antwerp, Belgium

Keywords: Au nanorods, electron tomography, DFT calculations, iodide ions, interface energy

The presence of iodide ions during the growth of gold nanorods strongly affects the shape of the final products, which has been proposed to be due to selective iodide adsorption on certain crystallographic facets. Therefore, a detailed structural and morphological characterization of the starting rods is crucial toward understanding this effect. Electron tomography was used to determine the crystallographic indices of the lateral facets of gold nanorods, as well as those present at the tips. Based on this information, we used density functional theory (DFT)

calculations to determine the surface and interface energies of the observed facets and provide insight into the relationship between the amount of iodide ions in the growth solution and the final morphology of anisotropic gold nanoparticles.

1. Introduction

Gold nanoparticles (Au NPs) are of great current interest, due to their unique electronic, optical, and catalytic properties, giving rise to applications in e.g. biomedicine, optoelectronics and photovoltaics.[1–3] The morphology of nanoparticles has a major effect on their physical properties. For example, the aspect ratio of gold nanorods (Au NRs) is a crucial parameter behind their optical behavior,[4] but other morphological details have also been shown to affect the frequency of localized surface plasmon resonances (LSPR) in Au NPs. Therefore, the ability to accurately tailor the final shape and size of Au NPs is of great interest. Much effort has been dedicated to develop synthesis methods under tightly controlled conditions, toward achieving this goal.[5–7] For example, various morphologies of Au NPs can be obtained, depending on the molar ratio of halide ions present during seeded growth. [8,9]

To understand the growth and stability of NPs down to the atomic scale, a combination of modeling and characterization techniques is required. Since the turn of the century, electron tomography has been used to investigate the 3D structure and shape of inorganic materials at the nanometer scale.[10,11] The technique derives a three-dimensional (3D) structure from a tilt series of two-dimensional (2D) projection images. Recently, it has even become possible to investigate the morphology of NRs with atomic resolution and in this manner the types of crystallographic facets at the surface of Au NRs have been indexed.[12] Computationally, DFT studies have been performed to study the environment-dependent growth for Au based nanosystems,[13] resulting for example in understanding the influence of the NP shape on CO adsorption.[14] The surface stability of Au surfaces in the presence of different halides has also been investigated by means of DFT simulations.[15] Preferential growth in a specific direction is hereby explained on the basis of the surface energies of different crystallographic facets and the effect of the adsorption of usual atomic and molecular additives on the surface stability.

We have previously reported the effect of iodide ions on the autocatalytic overgrowth of single-crystalline Au NRs.[16] For small amounts of potassium iodide (KI) in the solution, gold salt reduction was favored on the tips, leading to the formation of dumbbell-like NPs. Conversely, with an excess of iodide ions in the growth solution, the gold precursor reduction was found to be homogeneous, thereby preserving the initial shape of the rods upon overgrowth. It was suggested that the affinity of iodide toward gold causes the spontaneous replacement of bromide ions (from the employed surfactant), affecting the surface redox potential through the formation of AuI and AgI species. The formation of semiconducting halide species was proposed to catalyze the reduction of the gold precursor, in the presence of ascorbic acid (AA). The key argument was that the replacement of bromide by iodide was more efficient on the {111} facets at the tips than on the lateral parts. Therefore, at small amounts of iodide, the gold precursor would be reduced selectively on the tips, whereas at an excess of iodide the reduction could take place over the entire surface. By using advanced TEM with atomic scale resolution, we have now been able to determine the morphology of the initial Au NRs, as well as identify the crystallographic facets present at their tips. This information was used as an input for DFT calculations to provide insight into the relationship between different amounts of iodide in the growth solution and the final shape of the Au NPs. Since the shape of a nanostructure is determined by the surface energy as well as the contribution of the adsorption energy to the surface energy (which we shall from here on refer to as the interfacial energy), we calculated these energies for the relevant observed facets.

2. Synthesis

Prior to the overgrowth experiments, as-prepared Au NRs (**Figure 1)**, (see synthesis details in the experimental section) were washed to remove unreacted chemicals (AA, Ag^+) and the particles were re-dispersed in cetyltrimethylammonium bromide (CTAB) 0.1 M. To study the effect of iodide on the shape of the final particles, two experimental parameters were varied, namely the [KI]/[Au^0] and [Au^{3+}]/[Au^0] molar ratios. Regarding [KI]/[Au^0], we evaluated two molar ratios: 0.04 and 3.67, referred to as a low and high amount of iodide, respectively. For both iodide amounts, we performed overgrowth experiments for [Au^{3+}]/[Au^0] = 0.2 and 0.7, by keeping [Au^0] constant (0.15 mM) and varying the amount of added $HAuCl_4$. Therefore, for a given amount of iodide, the number of NPs did not vary.

3. Structural and morphological characterization

3.1 As-prepared Au NRs

We first investigated the as-prepared Au NRs by means of 2D and 3D high angle annular dark field scanning TEM (HAADF-STEM). Using electron tomography, the morphology could be reconstructed (Figure 1a) and a high resolution HAADF-STEM image of the same rod is shown in Figure S1. In order to determine the type of crystal facets at the surface, high resolution electron tomography was applied. We hereby used a previously developed methodology[12] in which four high-resolution HAADF-STEM images were acquired along different zone axes ([100], [110], [010] and [-110]) and subsequently combined by an algorithm that exploits the sparsity of the structure of the NRs at the atomic scale. In Figure 1b, one of the high resolution input images (acquired along a <110> axis) is shown. The remaining projection images are presented in Figure S2. In Figure 1c-e, 3D visualizations along different viewing directions and a slice through the reconstructed volume are presented. Although the reconstruction did not enable a direct indexing of the lateral facets due to surface roughness, the facets at the sides of the tip could be reliably investigated and were determined to correspond to {111} and {110} planes, in agreement with the findings reported in ref. [17].

3.2 Overgrown Au NRs

Next, pre-grown Au NRs, were used as seeds for overgrowth, in the presence of both low and high amounts of KI. Electron tomography was again applied on particles with varying amount of KI, indicating that, for a high KI content (by increasing the [Au^{3+}]/[Au^{0}] molar ratio), both the length and width of the initial nanorods (68.6±9.4 nm by 15.9±2.2 nm) progressively increased, to reach values of 73.5±6.8 and 24.4±1.9 nm, respectively. Importantly, the rod-like shape of the nanoparticles was preserved (**Figure 2 a-d**). On the contrary, for a low KI content, and increasing the [Au^{3+}]/[Au^{0}] molar ratio, the length increased up to 81.5±6.9 nm, while the width at the tips increased up to 25.7±3.1 nm. The width in the middle of the NRs however remained constant. These average dimensions were determined by analyzing more than 100 different NPs from low magnification TEM images (Figure S3). Such a region-specific gold reduction resulted in a dumbbell-like shape for the final NPs (Figure 2 e-h). This result, together with the information provided in Figure 1, is in agreement with our previous work.[16] This process yields final particles with a dumbbell shape.

4. Surface and interface energies

The as-prepared Au-NRs used in this study are identical to those investigated in previous work, where it was shown that the lateral facets are alternating {110}, {100} and {520} facets.[12] Here, we conclude that {110} facets are present at the sides of the tips as well, together with {111} planes, illustrated in Figures 1c and 1e respectively. This provides the input data required for DFT calculations. We therefore focus here on the surface energies and interfacial energies of {111}, {520} and {100} planes. The surface energy for each Au facet is calculated from the total energy of a slab with one relaxed surface ($E_{relaxed}^{tot}$) and the unrelaxed slab ($E_{Unrelaxed}^{tot}$), together with the total energy per atom in bulk gold (E_{bulk}^{tot}), which is given by

$$\gamma_{hkl} = \frac{\left(E_{Unrelaxed}^{tot} - N_{atom} E_{bulk}^{tot}\right)}{2\,A} + \frac{\left(E_{relaxed}^{tot} - E_{Unrelaxed}^{tot}\right)}{A} \tag{1}$$

where hkl represents the surface orientation, A the surface area and N_{atom} the total number of atoms in the considered slab. The calculated surface energies (γ_{hkl}) for {111}, {100}, and {520} Au facets were 1.169, 1.311, and 1.369 J/m^2, respectively. Since the overgrowth of Au NRs occurs in the presence of different amounts of I$^-$, it is important to further understand how the adsorption of iodide ions influences the stability of these different surfaces. We need to consider the contribution of the adsorption energy, i.e., the interface energies rather than the pure surface energies. When calculating the interface energy, the effect of the difference in adsorption energy of iodide on different crystallographic surfaces is also taken into account. For surfaces with many dangling bonds (such as the {520} facet), the surface energy is expected to be relatively high, but at the same time the adsorption energy of an atom/ion will be lower (i.e., more negative) which might result in a compensation effect.[13] The magnitude of this compensation effect in turn depends on the iodide concentration. As a result, a change in iodide concentration may induce a cross-over of the interfacial energies of the various facets and therefore the stabilities of the facets considered.

Considering N_{ads} iodine atoms (as adsorbates) on a Au surface with area A, the adsorption (E_{ads}) and interface (γ_{hkl}^{int}) energies are calculated as:

$$E_{ads}(I) = \frac{(E_{Slab+I}^{tot} - E_{Slab}^{tot} - N_{ads}E_{I}^{tot})}{N_{ads}} \tag{2}$$

$$\gamma_{hkl}^{int} = \gamma_{hkl} + \frac{N_{ads}E_{ads}}{A} \tag{3}$$

where E_{Slab+I}^{tot} and E_{Slab}^{tot} are the total energies of the slabs with and without adsorbed iodine atoms, and E_{I}^{tot} is the total energy of an isolated iodine atom. Experimentally, the adsorbate is an iodide ion (I$^-$) deposited on the Au surfaces. In our calculations, a neutral system (Au slab plus iodine atoms) is considered. Bader charges calculations show indeed that there is a strong charge transfer towards the adsorbed iodine atoms, effectively resulting in adsorbed iodide ions. We also considered a negatively charged system, which resulted in almost identical charges on the iodide ions while the remaining charges spread out over the metallic Au layers. Therefore, for our purpose, it is justified to perform the calculations for neutral systems. Additionally, this also avoids the convergence problem for the total energies of charged slab calculations. Many different configurations and concentrations of iodine atoms on Au slabs with {111}, {100}, and {520} surfaces were considered. We find the lowest adsorption energy for each surface by considering a single adsorbate on Au surface at different possible configurations such as on-top, bridge, and hollow sites before geometry optimization of the system. For the most stable configurations the interface energies as a function of iodine concentration are shown in **Figure 3**.

As mentioned above, the iodide concentration is experimentally found to critically determine the final nanoparticle shape, and thus the growth rate of the facets initially present. We correlate these findings to the calculated thermodynamic stability of these facets, as a function of iodide concentration. For low amounts of I atoms, the {111} surface is calculated to have the lowest interface energy. Experimentally, this is found to lead to dumbbell growth, which is in agreement with the computational result. By increasing the iodine concentration, the interface energies for all surfaces decrease due to the binding of iodine atoms to the surface. However, we observe that the interface energies γ_{520}^{int} and γ_{100}^{int} decrease faster with increasing I concentration than γ_{111}^{int}. This means that, as the iodide concentration increases, a departure from dumbbell growth towards rod-like growth should occur. This is indeed experimentally observed. A linear fit to our calculation data predicts that the {520} surface will have the lowest interface energy at a concentration of 0.04 iodine atom/Å^2. This corresponds to 1 iodine atom per 25 Å^2, which is before full coverage occurs.

In order to quantify the observed correlation between the theoretical findings and the experimental data, we estimated the number of I$^-$ ions per given area of the Au NR seeds. Taking the concentration of Au NRs in terms of [Au^0], which is equal to 0.15 mM, and the dimensions of the particles determined from TEM measurements (see above), we can estimate the number of seed NRs in the growth solution to be 1.12 x 10^{12}. By multiplying the number of NPs by the surface of one NR (1.46 x 10^{7} $Å^{2}$) we obtain the total available surface in the Au NR seeds (4.3 x 10^{17} $Å^{2}$). On the other hand, for low and high amount of KI in the growth solution, the number of I^- ions in the added solution is equal to 3.43 x 10^{16} and 3.31 x 10^{18}, respectively. Therefore, by correlating the I^- concentration with the available surface of metallic gold we could estimate that for low KI concentration, ca. 2 I^- ions are present per 25 $Å^{2}$ of metallic surface, whereas for high amount of KI, 190 I^- ions are adsorbed present per 25 $Å^{2}$, i.e., 2 orders of magnitude higher. For a given temperature, the amount of I^- ions adsorbed on the surface can thus be expected to be significantly higher at high KI concentration than at low KI concentration. We theoretically estimated that the threshold for the transition from dumbbell-to-nanorod overgrowth corresponds to one I^- ion adsorbed per 25 $Å^{2}$. The experimental data indicate that dumbbell-like overgrowth takes place at a slightly higher concentration of two I^- ions adsorbed per 25 $Å^{2}$. There is therefore a clear correlation between the calculated results and the experimental observations. The difference of a factor of two may result from the presence of other species. For example, the dumbbell like overgrowth is mediated by the presence of AgBr on the NRs surface. In the presence of KI, the displacement of Br^- by I^- leads to formation of AgI on the NRs surface, which in turns changes the surface redox potential of the seeds.

5. Conclusion

Depending on the amount of KI present during the overgrowth of single-crystalline Au NRs, either rod- or dumbbell-shaped particles can be obtained. The main reason for this is the higher efficiency of the replacement of bromide by iodide on the {111} facets, which were proposed in the past to be present at the tips. By using atomic resolution electron tomography we could confirm the presence of {111} facets at the sides of the tips. These results, together with information about the lateral facets, were used as input for the calculation of surface and interface energies, in order to explain the observed shapes and determine the correlation between changes in surface stability and iodide adsorption. These findings provide a significant insight into the overgrowth of Au NRs and we expect it to open new opportunities for the future characterization of similar systems, which are widely used in the field of plasmonics.

6. Experimental Section

Synthesis of materials: Cetyltrimethylammonium bromide (CTAB, ≥ 99.0 %), hydrogen tetrachloroaurate trihydrate ($HAuCl_4$, ≥ 99.9%), silver nitrate ($AgNO_3$, ≥ 99.0%), L-ascorbic acid (AA, ≥ 99.0 %), sodium borohydride ($NaBH_4$, ≥ 96.0%), hydrochloric acid (HCl, 37%) and potassium iodide (KI, ≥ 99.5 %) were purchased from Aldrich and used without further purification. Milli-Q water (resistivity 18.2 MΩ·cm at 25 °C) was used in all experiments. All glassware was washed with aqua regia, rinsed with Milli-Q water and dried before use.

Synthesis of Au NRs: Au NRs were prepared through the well-known seeded growth method,[18] based on the reduction of $HAuCl_4$ with ascorbic acid on CTAB-stabilized Au NP seeds (<3 nm), in the presence of CTAB, HCl, and $AgNO_3$. Au seeds were prepared by fast reduction of $HAuCl_4$ with $NaBH_4$ in CTAB solution. A certain volume of $HAuCl_4$ solution (25 µL, 0.05M) was added to a solution of CTAB (4.7 mL, 0.1 M) and then a freshly prepared $NaBH_4$ (300 µL, 10 mM) solution was rapidly injected under vigorous stirring. The solution color changed from yellow to brownish yellow and the stirring was stopped after 2 min. The Au seed solution was aged at room temperature for 30 min before use. Au NRs were grown by adding $HAuCl_4$ (1 mL, 0.05M) and HCl (1.9 mL, 1M) to a solution of CTAB (100 mL, 0.1M). The mixture was gently shaken and kept for 10 min at 30 ºC in a thermostatic bath. Afterwards, $AgNO_3$ solution (1.2 mL, 0.01M) was added to the mixture, which was gently shaken for few seconds, AA solution (0.8 mL, 0.1 M) was added to the growth solution and thoroughly shaken, turning colorless in few seconds. Finally, a certain volume of seeds solution (0.24 mL) was added and the solution vigorously shaken and then left undisturbed at 30 °C for 2 hours. Upon synthesis, the Au NRs solution (100 mL) was centrifuged (8000 rpm, 30 min) twice to remove excess $AgNO_3$, AA and HCl, and redispersed in CTAB solution (0.1 M). The final concentration of Au NRs in terms of Au was 5 mM.

Synthesis of overgrown NRs: For the overgrowth of Au NRs[16] in the presence of low or high amount of KI, a solution of CTAB (10 mL, 0.1 M) was mixed with an appropriate volume of $HAuCl_4$ (0.05M) and stored for 5 min at 30 ºC to allow for complexation of gold salt, followed by addition of KI (5.7 µL for low amount or 550 µL for high amount, 0.01 M) and an appropriate volume of AA (0.1 M) to maintain $[AA]/[Au^{+3}] = 1.6$. Finally, a Au NR seed solution (0.3 mL, 5 mM) was added under stirring. The mixture was left undisturbed at 30 °C for 30 minutes. To examine the influence of $HAuCl_4$ concentration (at constant $[KI]/[Au^0]$ molar ratio), different growth solutions were prepared with identical concentrations of CTAB (0.1 M), KI (5.7 µM – low, 550 µM - high), Au NRs (0.15 mM), and different $HAuCl_4$ concentrations chosen to fit the selected $[Au^{+3}]/[Au^0]$ molar ratios (0.2, 0.7). The $[AA]/[Au^{+3}]$ molar ratio was 1.6 in all experiments.

Experimental characterization: Low magnification tilt series for electron tomography were acquired by using an aberration-corrected cubed FEI Titan electron microscope operated at 300 kV. The series were acquired manually within a tilt range from -70^o to $+70^o$ and a tilt increment of 5^o by using a Fischione model 2020 single-tilt tomography holder. For the atomic resolution electron tomography analysis, four high-resolution HAADF-STEM images were acquired from one of the tips of a Au NR, along different zone axes ([100], [110], [010] and [-110]) by using a Fischione model 2040 tilt-rotation tomography holder. Prior to the tomographic reconstruction, these experimental images were drift compensated by using the known lattice proportions and angles between two planes at each specimen orientation.[19] Furthermore, the background of the images was subtracted and fitted as a 3D plane, and each image was also normalized in such a way that the sum of all pixel intensities was equal to one. For the tomographic reconstruction we used the simultaneous iterative reconstruction technique (SIRT) algorithm, with an additional constraint that at each iteration any negative reconstructed voxels are set to zero. This positivity constraint arises from the knowledge that our reconstructed object must be positive. However, it should be mentioned that no further assumptions are made concerning the positions of the atoms.

Modelling details: Calculations were performed using DFT as implemented in the VASP code.[20][21] VASP uses periodic boundary conditions to compute a solution to the Kohn–Sham equations within a plane-wave basis. The projector augmented wave (PAW) method[22] was used to represent the core electrons. The exchange-correlation interactions were approximated with the Perdew, Burke, and Ernzerhof (PBE) functional[23] and the van der Waals (vdW) density functional method of Tkatchenko and Scheffler (DFT-TS)[24] was employed. The Au (5d10 6s1), and I (5s2 5p5), electrons were treated as valence electrons. The electron wave functions were expanded with a plane wave basis set up to a cutoff energy of 400 eV, and the Brillouin zone of the 1×1 surface was sampled with a Monkhorst Pack grid of 9 × 9 × 1 k-point. The slabs were constructed with 4, 6, and 8 gold layers for (111), (100), and (520) surfaces and the vacuum separating subsequent slabs had about 14 Å width. Several 3×3×1 supercells were used to simulate the (111), (100), and (520) surfaces with 108, 144, and 192 atoms, respectively. The theoretical lattice constant of bulk gold is found to be 4.11 Å which is very close to the experimental value of 4.08 Å.

Supporting Information

Supporting Information is available from the Wiley Online Library or from the author.

Acknowledgements

This work was supported by the European Research Council (grant 335078 COLOURATOM to S.B.). T.A., S.V.A. S.B. and E.C.N., acknowledge funding from the Research Foundation Flanders (FWO, Belgium), through project funding (G.0218.14N and G.0369.15N) and a postdoctoral grant to T.A. L.M.L.-M. and M.G. acknowledge funding from the Spanish

Ministerio de Economía y Competitividad (grant MAT2013-46101-R). Mozhgan N. Amini and Thomas Altantzis contributed equally to this work.

Received: ((will be filled in by the editorial staff))
Revised: ((will be filled in by the editorial staff))
Published online: ((will be filled in by the editorial staff))

[1] X. Huang, S. Neretina, M. A. El-Sayed, *Adv. Mater.* **2009**, *21*, 4880.

[2] S. Lal, S. Link, N. J. Halas, *Nat. Photonics* **2007**, *1*, 641.

[3] Y. Lu, Y. Yin, Z. Li, Y. Xia, *Nano Lett.* **2002**, *2*, 785.

[4] J. Gao, C. M. Bender, C. J. Murphy, *Langmuir* **2003**, *19*, 9065.

[5] J. Pérez-Juste, I. Pastoriza-Santos, L. M. Liz-Marzán, P. Mulvaney, *Coord. Chem. Rev.* **2005**, *249*, 1870.

[6] S. Eustis, M. A. El-Sayed, *Chem. Soc. Rev.* **2006**, *35*, 209.

[7] L. M. Liz-Marzán, M. Grzelczak, *Science* **2017**, *356*, 1120.

[8] T. H. Ha, H. J. Koo, B. H. Chung, *J. Phys. Chem. C* **2007**, *111*, 1123.

[9] S. E. Lohse, N. D. Burrows, L. Scarabelli, L. M. Liz-Marzán, C. J. Murphy, *Chem. Mater.* **2014**, *26*, 34.

[10] P. A. Midgley, M. Weyland, *Ultramicroscopy* **2003**, *96*, 413.

[11] P. A. Midgley, R. E. Dunin-Borkowski, *Nat. Mater.* **2009**, *8*, 271.

[12] B. Goris, S. Bals, W. Van den Broek, E. Carbó-Argibay, S. Gómez-Graña, L. M. Liz-Marzán, G. Van Tendeloo, *Nat. Mater.* **2012**, *11*, 930.

[13] N. Almora-Barrios, G. Novell-Leruth, P. Whiting, L. M. Liz-Marzán, N. López, *Nano Lett.* **2014**, *14*, 871.

[14] G. D. Barmparis, I. N. Remediakis, *Phys. Rev. B - Condens. Matter Mater. Phys.* **2012**, *86*, 85457.

[15] H. Hu, L. Reven, A. D. Rey, *J. Phys. Chem. C* **2015**, *119*, 11909.

[16] M. Grzelczak, A. Sánchez-Iglesias, B. Rodríguez-González, R. Alvarez-Puebla, J.

Pérez-Juste, L. M. Liz-Marzán, *Adv. Funct. Mater.* **2008**, *18*, 3780.

[17] H. Katz-Boon, M. Walsh, C. Dwyer, P. Mulvaney, A. M. Funston, J. Etheridge, *Nano Lett.* **2015**, *15*, 1635.

[18] M. Liu, P. Guyot-Sionnest, *J. Phys. Chem. B* **2005**, *109*, 22192.

[19] A. De Backer, L. Jones, I. Lobato, T. Altantzis, B. Goris, P. D. Nellist, S. Bals, S. Van Aert, *Nanoscale* **2017**, *9*, 8791.

[20] G. Kresse, J. Furthmüller, *Phys. Rev. B* **1996**, *54*, 11169.

[21] G. Kresse, J. Furthmüller, *Comput. Mater. Sci.* **1996**, *6*, 15.

[22] P. E. Blöchl, *Phys. Rev. B* **1994**, *50*, 17953.

[23] J. Perdew, K. Burke, M. Ernzerhof, *Phys. Rev. Lett.* **1996**, *77*, 3865.

[24] A. Tkatchenko, M. Scheffler, *Phys. Rev. Lett.* **2009**, *102*, 73005.

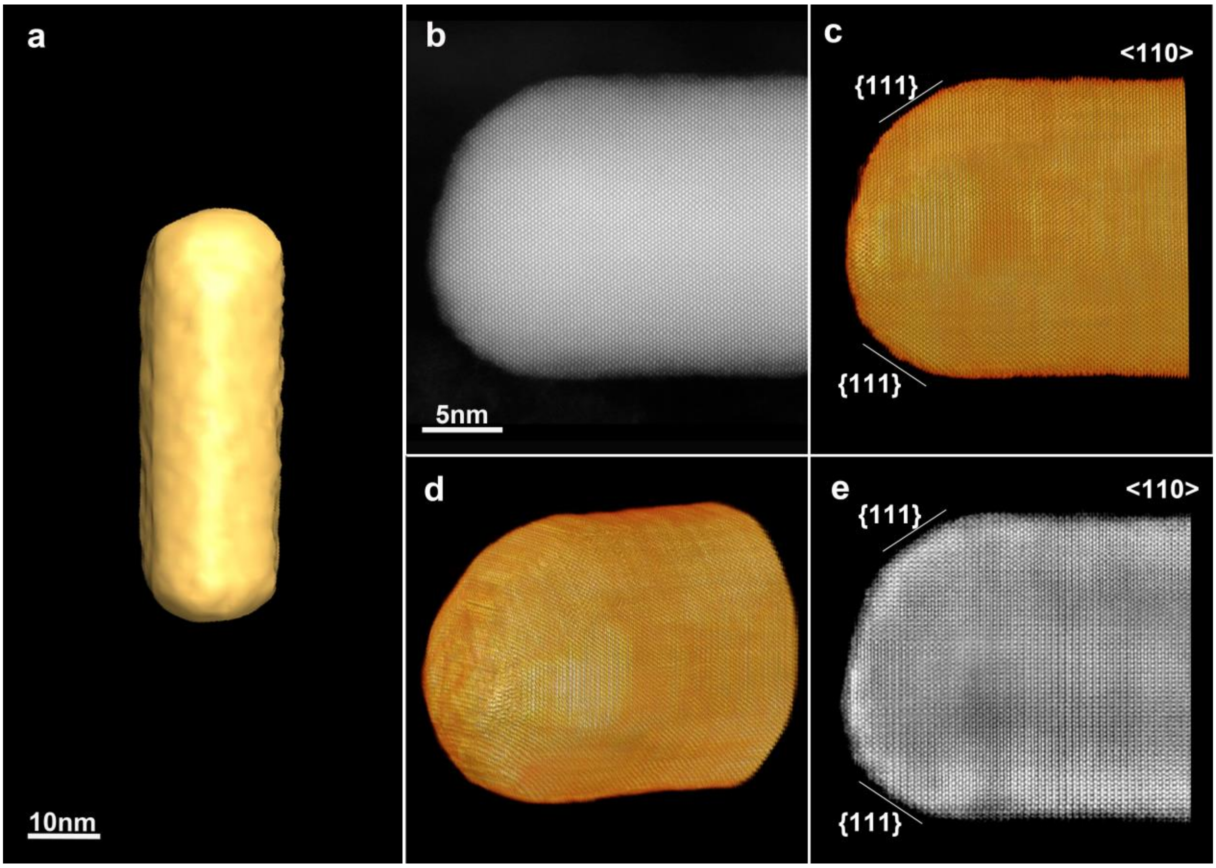

Figure 1. a) Morphology of an as-prepared Au NR, obtained by electron tomography, b) high resolution HAADF-STEM projection image from a part of a rod, oriented along [110]. c) and

d) 3D representation of the reconstructed volume along different viewing directions and e) an orthoslice through the volume shown in c. From this viewing direction it is clear that {111} facets are present at the sides of the tip.

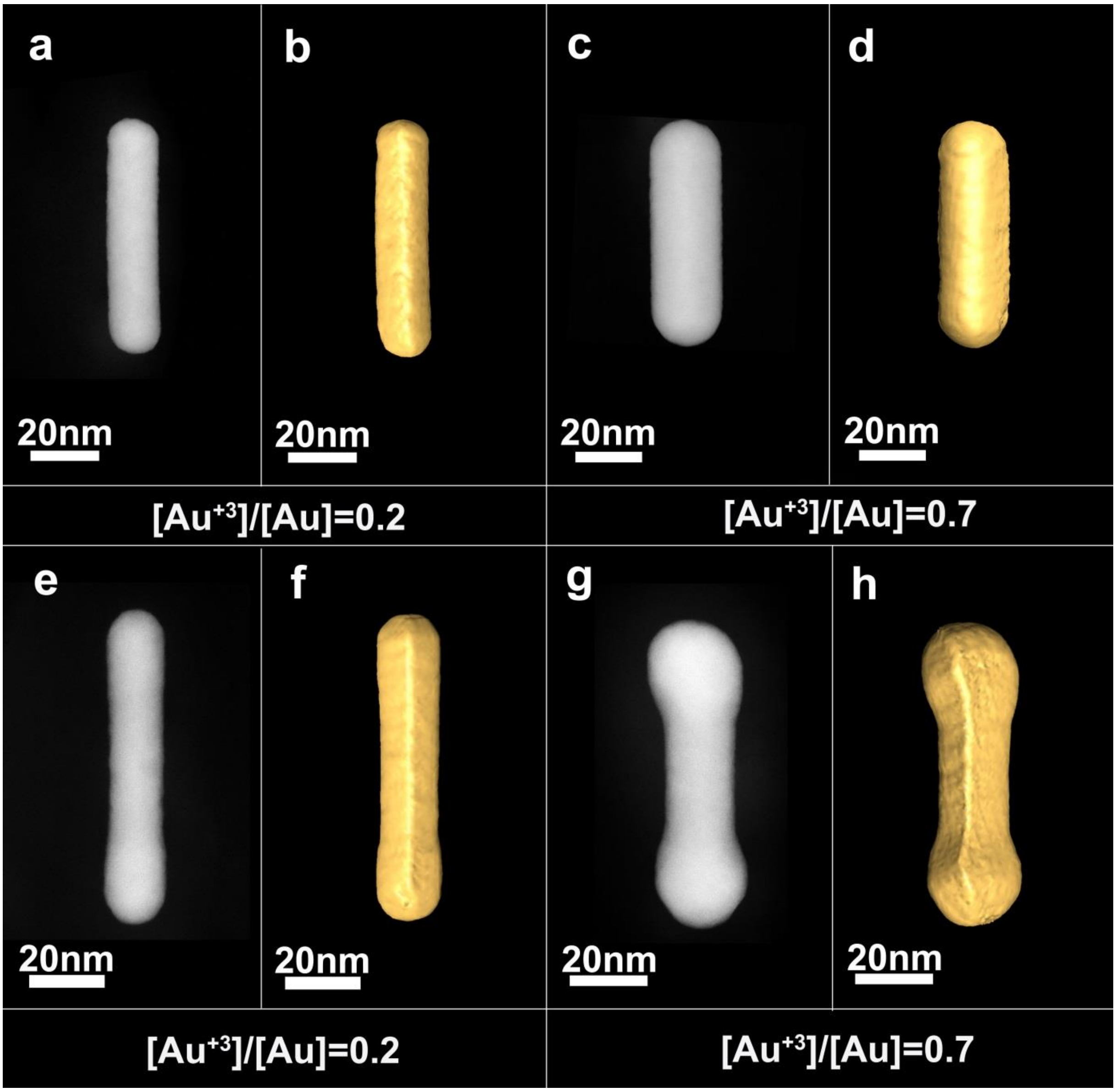

Figure 2. a-d) HAADF-STEM images together with 3D visualizations of the reconstructed volume, for rods of the samples overgrown in the presence of high amounts of KI and having a $[Au^{+3}]/[Au]$ molar ratio of a, b) 0.2 and c, d) 0.7 respectively. e-h) HAADF-STEM images together with 3D visualizations of the reconstructed volume, for rods of the samples overgrown in the presence of low amounts of KI having a $[Au^{+3}]/[Au]$ molar ratio of e, f) 0.2 and g, h) 0.7 respectively.

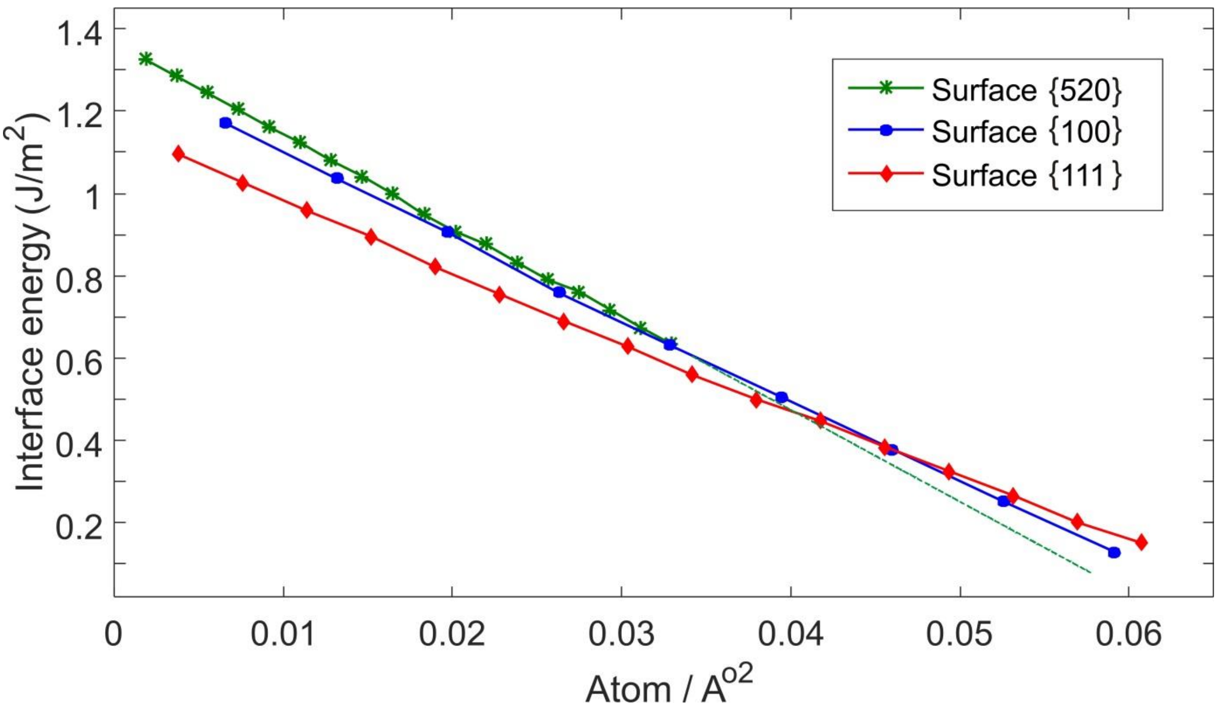

Figure 3. Interface energies as a function of the adsorbate density per surface for three Au facets.

Depending on the amount of KI present during the overgrowth of gold nanorods, either rod- or dumbbell-shaped particles can be obtained. Electron tomography and DFT calculations were employed to determine the crystallographic facets of gold nanorods and their surface and interface energies respectively, in order to unravel the relationship between the amount of I ions in the growth solution and the final morphology of anisotropic gold nanoparticles.

Keyword

Mozhgan N. Amini, Thomas Altantzis, Ivan Lobato, Marek Grzelczak, Ana Sánchez-Iglesias, Sandra Van Aert, Luis M. Liz-Marzán, Bart Partoens, Sara Bals* and Erik C. Neyts*

Understanding the Effect of Iodide Ions on the Morphology of Gold Nanorods

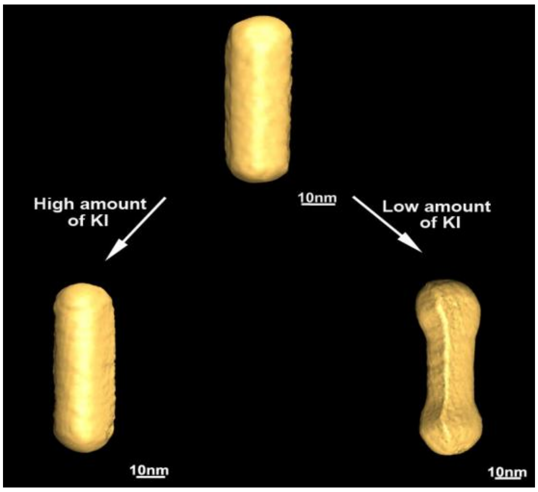

Supporting Information

for *Part. Part. Sys. Charact.*, DOI: 10.1002/ppsc.((please add manuscript number))

Understanding the Effect of Iodide Ions on the Morphology of Gold Nanorods

Mozhgan N. Amini, Thomas Altantzis, Ivan Lobato, Marek Grzelczak, Ana Sánchez-Iglesias, Sandra Van Aert, Luis M. Liz-Marzán, Bart Partoens, Sara Bals and Erik C. Neyts**

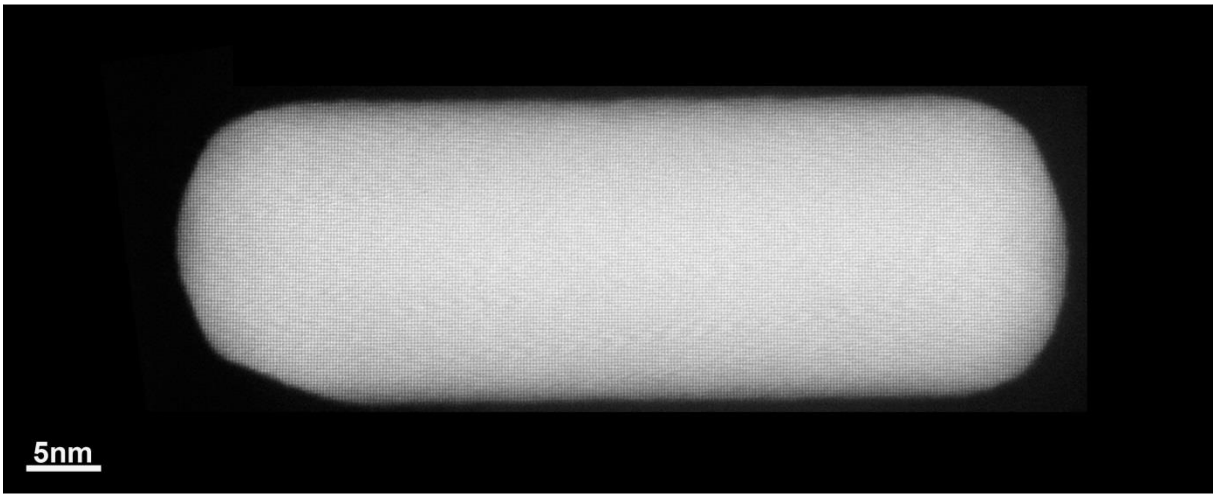

Figure S1. High resolution HAADF-STEM projection image of the as-prepared Au-NR, used for the acquisition of low magnification electron tomography series.

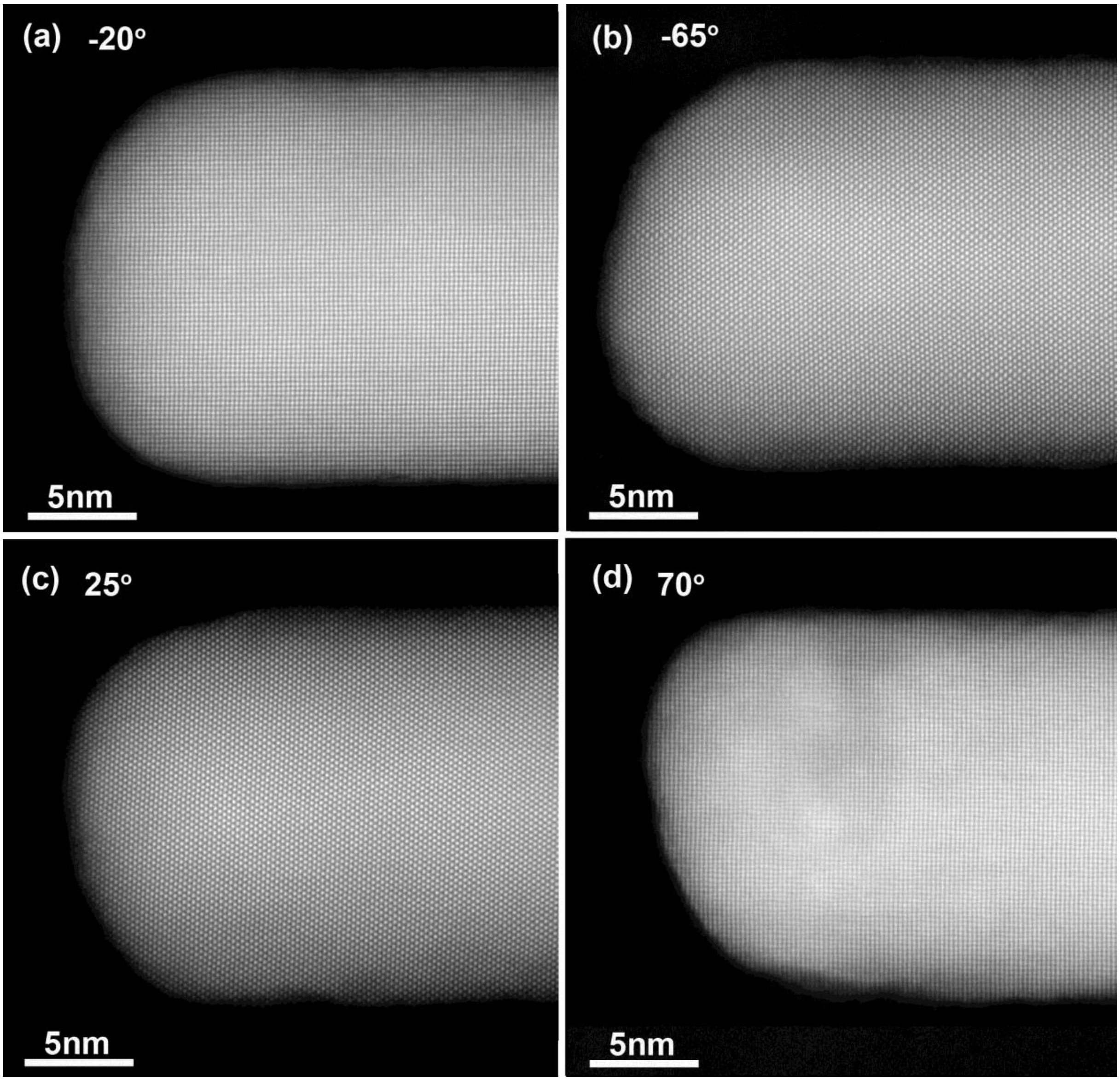

Figure S2. a-d) High resolution HAADF-STEM projection images from a tip of a rod, used for the acquisition of atomic resolution electron tomography series, along four different zone axis.

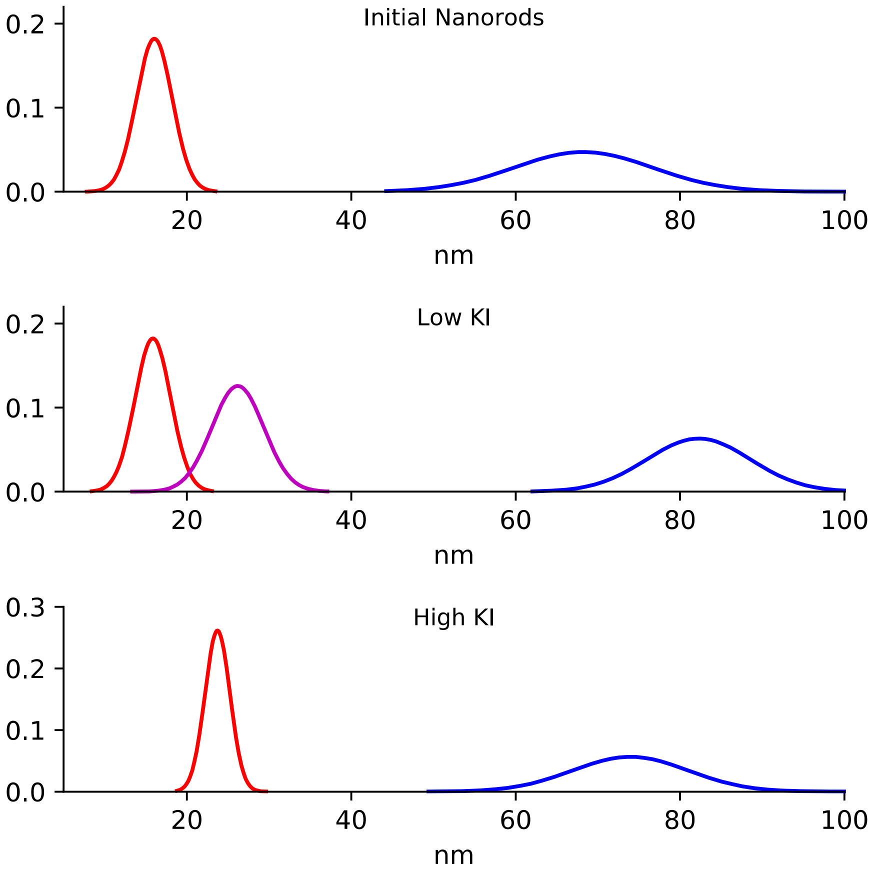

Figure S3. Size distributions of initial NRs (upper), grown at low amount of KI (middle) and at high amount of KI (bottom). Color code: width at the middle (red), width at the tips (magenta) and length (blue).